MATERIALS CHEMISTRY

FRONTIERS







RESEARCH ARTICLE

View Article Online



Cite this: Mater. Chem. Front., 2019. 3. 1642

Jeromy J. Rech, particular Nicole Bauer, particular David Dirkes, particular, Joseph Kaplan, a Zhengxing Peng, 🌘 b Huotian Zhang, 📭 c Long Ye, 📵 b Shubin Liu, 📵 d Feng Gao, Och Harald Ade Ob and Wei You **

ring electron acceptors in organic solar cells†

The crucial role of end group planarity for fused-

Newly developed fused-ring electron acceptors (FREAs) have proven to be an effective class of materials for extending the absorption window and boosting the efficiency of organic photovoltaics (OPVs). While numerous acceptors have been developed, there is surprisingly little structural diversity among high performance FREAs in literature. Of the high efficiency electron acceptors reported, the vast majority utilize derivatives of 2-(3-oxo-2,3-dihydroinden-1-ylidene)malononitrile (INCN) as the acceptor moiety. It has been postulated that the high electron mobility exhibited by FREA molecules with INCN end groups is a result of close $\pi-\pi$ stacking between the neighboring planar INCN groups, forming an effective charge transport pathway between molecules. To explore this as a design rationale for electron acceptors, we synthesized a new fused-ring electron acceptor, IDTCF, which has methyl substituents out of plane to the conjugated acceptor backbone. These methyl groups hinder packing and expand the $\pi-\pi$ stacking distance by ~ 1 Å, but have little impact on the optical or electrochemical properties of the individual FREA molecule. The extra steric hindrance from the out of plane methyl substituents restricts packing and results in large amounts of geminate recombination, thus degrading the device performance. Our results show that intermolecular interactions (especially $\pi-\pi$ stacking between end groups) play a crucial role in performance of FREAs. We demonstrated that the planarity of the acceptor unit is of paramount importance as even minor deviations in end group distance are enough to disrupt crystallinity and cripple device performance.

Received 16th May 2019, Accepted 17th May 2019

DOI: 10.1039/c9qm00314b

rsc.li/frontiers-materials

Introduction

The efficiency of bulk heterojunction (BHJ) organic photovoltaics (OPVs) has recently observed a surge in record high efficiency (over 16% for single junction and over 17% for tandem devices),1-8 largely from the emergence of non-fullerene acceptors (NFAs). 1-3,6,9-13 Along with the benefits of solution processability, low cost, and semi-transparency, OPV blends with NFAs can now achieve efficiencies higher than those of fullerene-based blends due to their complementary absorption and tunable energy levels. 14-21 The most common class of NFAs are fused-ring electron acceptors (FREAs), which have a characteristic acceptordonor-acceptor (A-D-A) architecture, such as ITIC (i.e., 3,9-bis(2methylene-(3-(1,1-dicyanomethylene)-indanone))-5,5,11,11-tetrakis-(4-hexylphenyl)-dithieno[2,3-d:2',3'-d']-s-indaceno[1,2-b:5,6-b']dithiophene). 11 ITIC was first reported by Xiaowei Zhan's group in 2015, and this publication helped catalyze the synthesis of many new FREAs. In fact, ITIC and its derivatives have become the center of focus for many research groups. 6,22-28

While device efficiencies have shown great improvement, the structural changes in new FREAs have become increasingly minor and the locations for new functionalization are becoming sparse. In short, the field has become saturated with ITIC and its derivatives, which has limited the synthesis of new and novel structures. In particular, the acceptor moiety, 2-(3-oxo-2,3-dihydroinden-1-vlidene)malononitrile (INCN), has only seen minor development. However, it is important to note that some of these changes have shown substantial improvements in the BHJ device efficiency, such as IT-M and IT-4F, 29,30 compared to the original ITIC. Indeed, these works have pushed the efficiency levels forward in great strides, but to continue forward at this pace, new materials will need to be explored, and understanding

^a Department of Chemistry, University of North Carolina at Chapel Hill, Chapel Hill, NC 27599, USA. E-mail: wyou@unc.edu

^b Department of Physics and Organic and Carbon Electronics Lab (ORaCEL), North Carolina State University, Raleigh, NC 27695, USA

^c Biomolecular and Organic Electronics, IFM, Linköping University, Linköping 58183, Sweden

^d Research Computing Center, University of North Carolina at Chapel Hill, Chapel Hill, North Carolina 27599-3420, USA

[†] Electronic supplementary information (ESI) available: π - π stacking literature survey, material synthesis and characterization procedures, device fabrication and optimization results, computational results and packing with XRD, recombination and transport studies with light intensity and photoluminescence experiments. See DOI: 10.1039/c9qm00314b

Research Article

Analyzing the shared structural features of notably highperforming FREAs can offer clues on the molecular engineering requirements. These include: (a) A-D-A architecture for tunability of band gap and energy levels; (b) conjugated ladder core to serve as an intermolecular charge transport channel; (c) alkyl side chains connected to a tetrahedral carbon on the donor unit to increase solubility, processability, and prevent excessive aggregation; (d) planar exposed electron deficient end groups that can form charge transport channels with neighboring acceptor molecules, presumably via the end-group interaction between different FREAs. 14-21,27,31-34 However, a more in-depth understanding of these requirements is lacking. For example, there have been many studies on the synthesis and performance of new FREAs, 1,12,13,23,35-43 but little work has focused on the molecular packing of these materials (i.e., requirement (d) above). To obtain high efficiency, OPV electron acceptors need a high electron mobility in order to extract electrons from the active layer and transport them to the cathode before they recombine. It is thought that the high electron mobility exhibited by small molecule NFAs is a result of close π - π stacking between neighboring acceptor end groups, which facilitate intermolecular π -orbital interactions and form charge transport pathways across neighboring NFA molecules. 27,31

Based on the shared structural features, a few groups have proposed diagrams to show the molecular packing of FREAs;^{32–34} however, the direct observation and limits of these models have often not been tested. For example, charge transport between acceptors is believed to occur at the FREAs acceptor end groups, and the distance between acceptor end groups (i.e., π – π stacking distance) needs to be sufficient for charge transport to occur. Values for efficient charge transport are often estimated to be within the 3-4 Å range, but most models don't offer further insight on this distance requirement. These models come in part from grazing-incidence wide-angle X-ray scattering (GIWAXS) measurements, which typically show lamellar and π - π stacking in FREAs, but this information alone lacks the details needed for a complete understanding. Very recently, Lu and co-workers used measurements such as GIWAXS to experimentally illustrate the formation of charge transport pathways via the interactions of the INCN end groups of ITIC and ITIC-Th. 44 This work serves as a strong example to validate the design of such models. While each model shows this favorable π - π stacking of the INCN end groups as the charge pathway between two acceptors, none include the limits of this interaction (i.e., maximum π - π stacking distance possible while maintaining efficient charge transport). Understanding the limits of the packing is important to the design of new NFAs, as clear structural design criterion can streamline the development of new high performance FREAs.

As previously mentioned, there was no strict consensus on the specific values of distance that FREAs would have to reach in order to achieve high performance in OPVs; thus, we conducted a quick literature survey of a large variety of high performance FREAs, $^{1,23,28,35,36,45-65}$ and organized the data on π - π stacking distance in Fig. 1a. The π - π stacking distance was reported for each of these materials through crystal structure, neat XRD, or GIWAXS measurement, and a table summarizing these values along with the chemical structures of each FREA is shown in the ESI† (Table S1 and Fig. S1). It is important to note that these values come from the neat, small molecule only films; once blended with a donor polymer, the range of π - π stacking distances varies based on the miscibility and interaction between the components of the active layer. Nevertheless, Fig. 1a clearly shows that high performance FREA-based blends reported in literature display a close π - π stacking distance of \sim 3.5 Å between acceptor end units forming the charge transport pathways. This very narrow distribution of distance between end groups of these FREAs, centering around 3.5 Å, presents an interesting and important question: Is this distance, ~ 3.5 Å, a prerequisite or key criterion in designing new FREAs? Or, if everything else was equal, would a significant deviation from this distance of 3.5 Å lead to a decrease in photovoltaic performance? To address these questions, we designed a new sterically hindered FREA (i.e., IDTCF, structure in Fig. 1b) which would have a π - π stacking distance outside the range shown by current

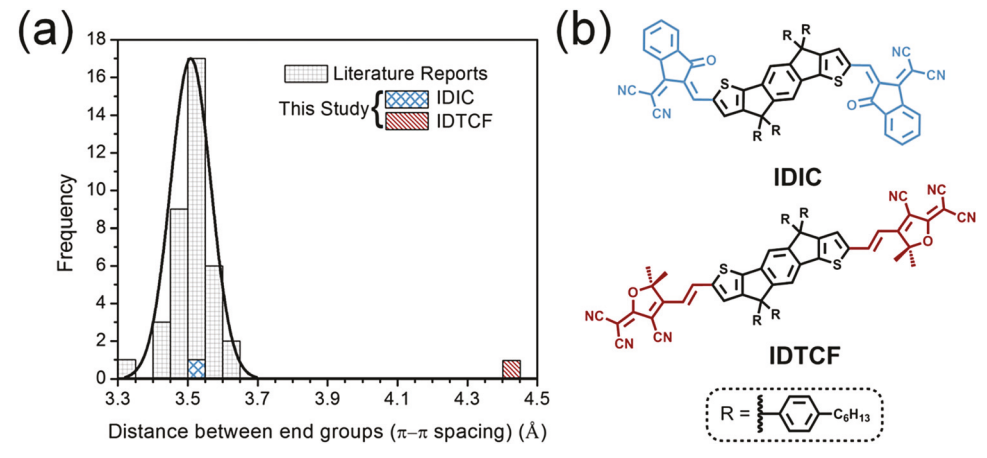


Fig. 1 (a) Histogram of $\pi-\pi$ spacing distances reported in literature of high performance FREAs and (b) chemical structures of fused-ring electron acceptors: IDIC and IDTCF.

high performance FREAs (\sim 3.3 Å to \sim 3.7 Å). By further studying the tolerance with the end group interaction, a sharper understanding of the molecular design requirements can help facilitate the design of new high performance NFAs.

Herein, we present two FREAs, IDIC and IDTCF (structures in Fig. 1b), with distinct chemical structures that produce different π - π stacking distances between the FREA end groups and show that the chemical structure of the end groups are indeed responsible for the π - π stacking distances seen in these FREAs. The increased stacking distance was expected to have a strong limit on the end group interaction, which would significantly impact the device performance. IDTCF is a new A-D-Atype FREA which consists of an indacenodithiophene (IDT) donor core and two tricyanovinyldihydrofuran (TCF) acceptor end groups. Unlike the INCN end group in the case of IDIC, the TCF end group in IDTCF has two methyl substituents which are out of the plane of the backbone, making it more difficult for the IDTCF to pack closely. Given the same IDT core and A-D-A structure, IDIC and IDTCF have similar optical and electrochemical properties, but IDTCF has a larger intermolecular π - π stacking distance (4.40 Å) due to steric hindrance from the outof-plane methyl substituents. The hindered packing of IDTCF extends the minimum packing distance by ~1 Å; however, the device performance for the IDTCF-based OPV device is drastically $(\sim 10 \times)$ lower than that of IDIC-based one. The origin of the different efficiencies for each acceptor was carefully analyzed, and our results clearly manifest the importance of close π – π stacking distance and planarity of the end groups of FREAs, providing an important design criterion to consider when developing new FREAs for higher device efficiencies.

Results and discussion

Materials

The chemical structure for each acceptor material in this study is depicted in Fig. 1b, and the full synthetic route for each of the FREAs (IDTCF and IDIC) is shown in Fig. S2 (ESI†). The indaceno-dithiophene (IDT) core, INCN, and TCF acceptor end groups were synthesized according to previous literature reports, 11,39,66 and a Knoevenagel condensation between IDT and INCN or TCF

afforded the IDIC or IDTCF in 75% and 52% yields, respectively. The structure of each FREA was confirmed by nuclear magnetic resonance (NMR) (Fig. S3 and S4, ESI†) and mass spectroscopy (see ESI†), and each FREA showed good solubility in common solvents such as chloroform, toluene, and chlorobenzene.

Photovoltaic performance

We first explored the relationship between photovoltaic performance and end group stacking distance by pairing each acceptor with a wide bandgap donor polymer, FTAZ,67 in bulk heterojunction (BHJ) solar cells. Devices were prepared with an inverted architecture of ITO/ZnO/FTAZ:acceptor/MoO₃/Al, a donor: acceptor (D:A) ratio of 1:1, and chlorobenzene as the solvent. Details of solvent optimization can be found in Table S2 (ESI†). Representative J-V curves are displayed in Fig. 2a, and the photovoltaic characteristics are outlined in Table 1. From these results, it is clear that the IDIC-based devices outperform those based on IDTCF. IDIC-based devices show a higher short-circuit current density (J_{sc}) , open-circuit voltage (V_{oc}) , and fill factor (FF), leading to an overall power conversion efficiency (PCE) nearly ten times greater than that of the IDTCF-based ones. The external quantum efficiency (EQE) of each blend was also measured, and is shown in Fig. 2b. Both devices have a broad EQE response; however, FTAZ:IDIC has a much higher EQE response than FTAZ:IDTCF, with maximum values reaching ~55% and $\sim 15\%$, respectively.

We also synthesized two additional FREAs with an indacenodithienothiophene (IDTT) core, yielding ITIC and ITTCF, whose chemical structures are shown in Fig. S5a (ESI \dagger). From the J–Vcurves, shown in Fig. S5b (ESI \dagger), with each of these new FREAs paired with FTAZ in BHJ solar cells, it is clear that the same decrease in performance is seen for all materials with the hindered TCF acceptor moiety. This finding can eliminate any performance decrease due to the choice in the donor core.

From these results, it is clear that the structural changes in IDTCF (*i.e.*, compared with the structure of IDIC) are detrimental to the performance of BHJ solar cells, likely due to the hindered packing of the TCF end groups (the only structural difference between IDTCF and IDIC). To further corroborate this claim and disclose more detailed structure–property correlation, we explored

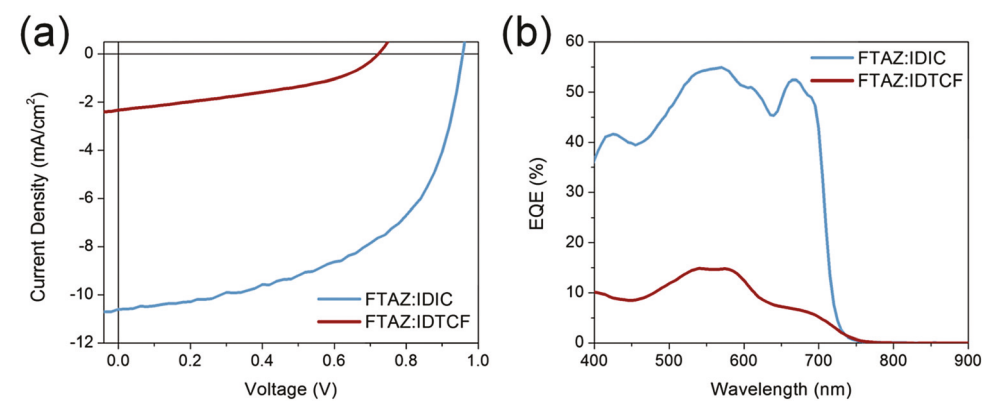


Fig. 2 (a) Representative J-V curves and (b) EQE spectra for the FTAZ:IDIC and FTAZ:IDTCF devices.

Acceptor	$J_{ m sc}~({ m mA~cm}^{-2})$	$V_{\rm oc}$ (V)	FF (%)	PCE (%)
IDIC IDTCF	$10.79 \pm 0.18 \\ 2.10 \pm 0.12$	$\begin{array}{c} 0.954 \pm 0.004 \\ 0.705 \pm 0.034 \end{array}$	50.6 ± 1.5 39.6 ± 1.8	$5.21 \pm 0.19 \\ 0.59 \pm 0.06$

the electrochemical, optical, and morphological properties of each FREA.

Electrochemical properties

Research Article

We first investigated the electrochemical properties of these materials, using cyclic voltammetry (CV) to measure their highest occupied molecular orbital (HOMO) and lowest unoccupied molecular orbital (LUMO) levels. The CV curves are displayed in Fig. 3a, and the energy levels are summarized in Fig. 3b. As there is a decrease in $V_{\rm oc}$ for the IDTCF-based device, and the $V_{\rm oc}$ is generally related to the energy difference between the LUMO of the acceptor and the HOMO of the donor, an understanding of these energy levels would provide insight into this decrease of $V_{\rm oc}$. However, both FREAs have a similar LUMO level (-3.99 eV for IDIC and -3.98 eV for IDTCF), which would suggest that the lower $V_{\rm oc}$ and performance for the IDTCF-based device is not due to a difference in energetics, but to some other underlying cause. This V_{oc} loss will be further discussed in the charged transport section.

Optical properties

To explore the decrease in the J_{sc} for the IDTCF-based device, we studied the optical properties of the FREAs. The absorption spectra for IDIC and IDTCF in solution and thin films are shown in Fig. S6a (ESI†) and Fig. 3c, respectively. The IDIC molecule shows a strong intramolecular charge transfer (ICT) band at 682 nm, with weaker shoulder absorption at 620 nm. Meanwhile, the IDTCF molecule shows a broader absorption with a maximum absorbance at 610 nm. The full width at half maximum (FWHM) for IDIC and IDTCF are 106 nm and 184 nm, respectively. We previously claimed the methyl substituents on the acceptor moiety of the IDTCF molecule increase the steric hindrance and make packing more difficult, which would lead to a large ensemble of orientations

which are present for IDTCF at any given point in time, as illustrated by the 1.7 times larger FWHM. Conversely, the IDIC has a more crystalline structure, resulting in fewer conformations, and therefore a smaller FWHM. Nevertheless, both FREAs have similar optical bandgaps, determined by the absorption onset, which helps corroborate the claim that the TCF and INCN end groups have similar electron withdrawing strength.

The donor polymer, FTAZ, on the other hand, has the strongest absorbance from 400-600 nm, which is complementary to the absorption of the IDIC molecule. The IDTCF molecule, however, has more overlap in its absorption with that of FTAZ. This is further illustrated in the entire device absorbance, shown in Fig. S6b (ESI†). While there is less absorbance in the range beyond 600 nm for IDTCF blend, the absorption coefficient of both the FTAZ:IDTCF and FTAZ:IDIC are similar across the entire range. Therefore, absorption difference alone cannot account for the observed huge difference between the J_{sc} value of the FTAZ:IDTCF device and that of the FTAZ:IDIC one (Table 1). In fact, the much diminished EQE response in the region of 400 nm to 600 nm in the FTAZ:IDTCF device (Fig. 2b) where the FTAZ polymer would contribute the most - indicate that there would exist significant issues with either charge generation, charge transport, or both in the FTAZ:IDTCF device.

Computational modeling

To further understand the interactions between the electron acceptors, we utilized computation and modeling to explore the closest packing of both FREAs. We performed density functional theory (DFT) calculations at the DFT wB97XD/6-31G(d) level of theory using Gaussian 16 package, version A03. We modeled both a single FREA molecule and a dimer system for both IDIC and IDTCF, and to reduce the computation time yet still maintain the chemical structure, the hexyl side chain was replaced with a methyl substituent. Fig. S7a and c (ESI†) represent the most stable conformation of both the single units, and the methyl substituents of TCF are highlighted in red. The IDTCF has a minimum energy conformation which is planar, as illustrated in Fig. S7c (ESI†), while the IDIC has a slight bending at the end groups. However, in the dimer system of IDIC, this slight twist is

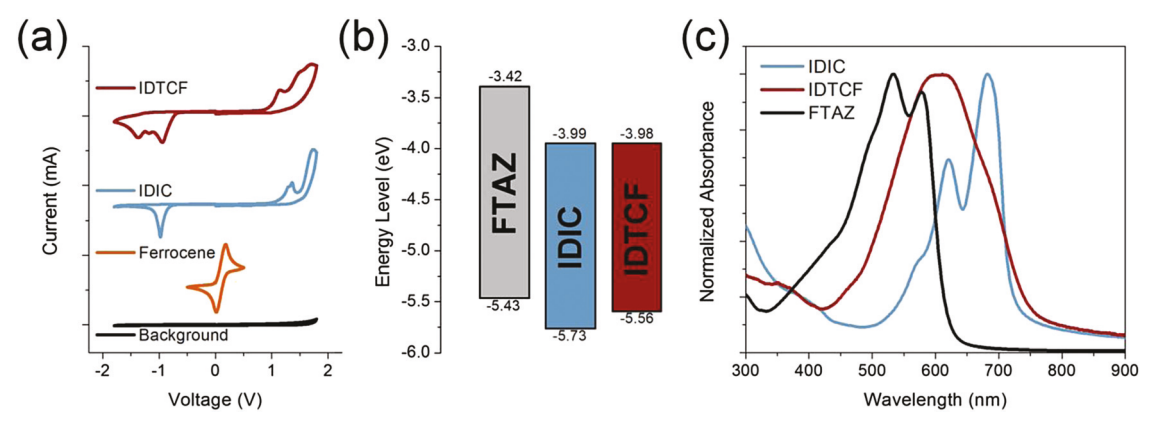


Fig. 3 (a) Electrochemical measurements of HOMO and LUMO through cyclic voltammetry, (b) HOMO/LUMO energy diagram from CV results, and (c) thin film UV-visible absorbance spectrum of each of the materials studied.

matched by the next acceptor unit, which allows the IDIC molecules to tightly pack. Fig. S7b (ESI†) shows the dimer system for IDIC, and the distance between the INCN end groups was calculated to be 3.58 Å. This value is further corroborated within literature reports, where GIWAXS measurements of films of neat IDIC show an in-plane (IP) π - π stacking distance of 3.45 Å.³⁹ In the dimer system of IDTCF, shown in Fig. S7d (ESI†), the FREAs show more twisting and an expanded π - π stacking distance of 3.84 Å. It is important to note that this is the closest packing that is possible for the IDTCF acceptors, and the distance between end groups can be even larger in real films. Additionally, this modeling was only done with a dimer system, so the effects from more IDTCF molecules are unknown.

Furthermore, the computed electron distributions at the ground and excited states of both FREAs are provided in Fig. S8 (ESI†). The electron distributions, showing the HOMO and LUMO energy levels, for both IDIC and IDTCF show a similar distribution of electron density across each molecule, which further confirms the previous claim that both FREA end groups have similar electron withdrawing strength when paired with the IDT core.

Packing of molecules in thin films

If there is a difference in the packing, as indicated by the previous DFT calculations, we would expect to see a difference in the order and crystallinity of the materials. The hindered IDTCF small molecule was unable to form appropriate single crystals for analysis, so we utilized X-ray diffraction and GIWAXS measurements to explore these properties. We began by performing X-ray diffraction (XRD) measurements of spuncast samples for each of the neat small molecule films, as illustrated in Fig. S9 (ESI†). To begin with, Fig. S9a (ESI†) is the out-of-plane (OOP) XRD scan for each FREA. For IDIC, we identified two lamella scattering peaks at 3.3° and 5.0° two theta peaks shown in Fig. S9a (ESI†). This further confirms the packing and semi-crystalline nature of IDIC. In contrast, IDTCF shows no scattering signal in the OOP direction. This lack of signal helps further support the claim that the out-of-plane methyl substituents on the TCF end group disrupt the packing required for efficient charge transport. Next, Fig. S9b (ESI†) is the in-plane (IP) XRD scan for each FREA. Similar to the OOP scan, IDTCF shows no peaks, which again suggests no ordering in the film. In the case of IDIC, a small peak is observed; however, the XRD signal which would corresponds to π - π stacking, was not identified. Overall, the XRD data clearly illustrates a loss of ordering for the FREA containing the hindered TCF group, further supporting the claim that IDTCF is unable to pack and form charge transport pathways.

To confirm the larger π – π stacking distance, we also measured the molecular packing and texture through synchrotron radiation-based GIWAXS.⁶⁸ We previously reported both neat IDIC and FTAZ:IDIC blends with GIWAXS,³⁹ and the neat IDTCF and blend with FTAZ are shown in Fig. 4. In the neat IDTCF case, the GIWAXS pattern illustrates a random orientation for IDTCF, as shown by the diffuse halo in Fig. 4a, which further corroborates the XRD data. The π – π stacking is shown by the (010) peak in the OOP, at $q=1.43~\text{Å}^{-1}$, corresponding to a 4.40 Å π – π stacking distance.

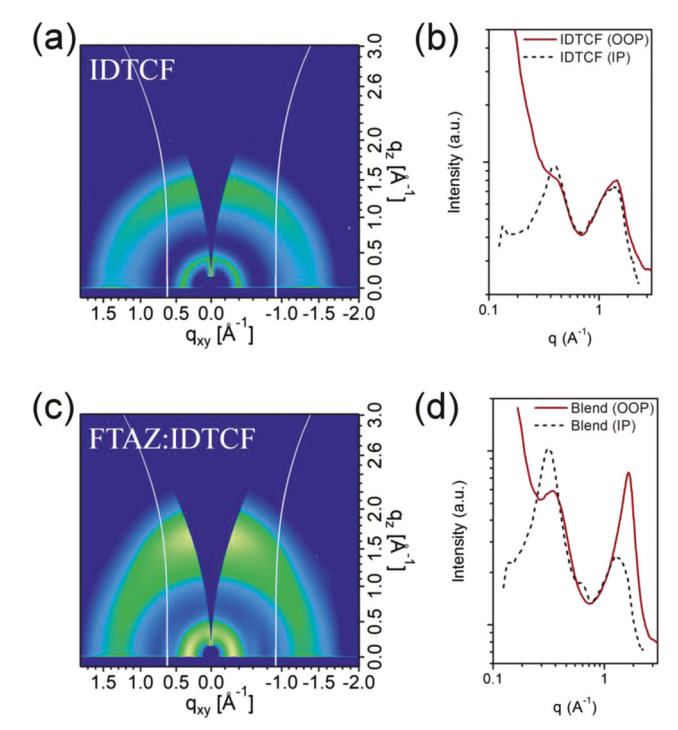


Fig. 4 (a and c) 2D GIWAXS patterns and (b and d) in-plane (IP) and out-of-plane (OOP) profiles of neat IDTCF film and FTAZ:IDTCF blend film.

This value is significantly larger than that of the (010) peak of IDIC, at $q=1.82~\text{Å}^{-1}$ peak, which corresponds to a $\pi-\pi$ stacking distance of 3.45 Å. Additionally, when IDTCF is blended with FTAZ (Fig. 4c and d), the (010) peak of the blend system shifts to $q=1.38~\text{Å}^{-1}$, which corresponds to a $\pi-\pi$ stacking distance of 4.56 Å.

The next interesting point is to look at the changes that occur to the packing of FTAZ when blended with IDTCF. In the in-plane blend film, the FTAZ contributes to the signals at $q=0.32~\text{Å}^{-1}$ and $q=0.63~\text{Å}^{-1}$, which are (100) and (200) peaks. In the OOP direction, when FTAZ is blended with a high performance non-fullerene acceptor, the (010) peak was located between $q\sim1.7-1.8~\text{Å}^{-1}$ (3.5–3.7 Å), 13,40,42,69,70 however, for the FTAZ:IDTCF blend film, the (010) peak is shifted to $q=1.65~\text{Å}^{-1}$, which corresponds to a larger π - π stacking distance of 3.81 Å. This illustrates that the IDTCF acceptor also disrupts the packing of FTAZ, which may lower the hole mobility of FTAZ (*vide infra*).

The GIWAXS results clearly illustrate that the end group packing is expanded by ~ 1 Å from the out of plane methyl substituents of TCF, and compared to the materials outlined in the literature survey conducted at the beginning of this work, the 4.40 Å π – π stacking distance of IDTCF is outside the range seen in high performance FREAs. Additionally, as both IDIC and IDTCF have similar optical and electrochemical properties, with the only difference being the additional sterics of the TCF acceptor group, we show the importance of the planarity of the end group acceptor moieties and the impact on device performance.

Charge transport

While IDIC and IDTCF have stark differences in device performance (e.g., J_{sc} , V_{oc} , and FF), their optical and electrochemical

properties are similar, indicating that inferior charge transfer and/or charge transport in the IDTCF-based device may be causing the lower performance; each of which can be attributed to the inferior packing which was outlined in the previous section. In many OPV systems, bimolecular recombination has been shown to be the dominant recombination mechanism, thus limiting charge transport and efficiency. 71-73 Furthermore, we have established that the IDTCF molecules have poor packing attributed to the out-of-plane methyl substituents, which could lead to recombination issues. One technique to probe the recombination mechanism is to look at the light intensity dependence of both J_{sc} and V_{oc} . It has been established that the slope value (m) of the light intensity plots can help elucidate the key recombination mechanisms present in the solar cell.⁷⁴ For example, in a semi-log plot of V_{oc} vs. light intensity, a slope of 1 kT/q indicates that bimolecular recombination is the major loss mechanism under open-circuit conditions. Values less than 1 kT/q signify surface recombination, ^{75,76} and as the slope approaches 2 kT/q, trap-assisted recombination becomes the dominant recombination mechanism.77,78 In Fig. S10b (ESI†), the slopes for both the FTAZ:IDIC and FTAZ:IDTCF blends are very close to 1 kT/q, which indicates that bimolecular is dominant in terms of non-geminate recombination mechanisms. Next, J_{sc} is known to have a power law dependence on light intensity, such that the slope of the log-log plot of $J_{\rm sc}$ vs. light intensity indicates the strength of bimolecular recombination under short-circuit conditions. When the slope is close to unity, only weak bimolecular recombination is present, which is what we find for both FTAZ:IDIC and FTAZ:IDTCF blends in Fig. S10a (ESI†). Consequently, the light intensity data in Fig. S10 (ESI†) illustrate that both IDIC and IDTCF containing blends have very similar and low bimolecular recombination. This unexpected result suggests that the issue may be with geminate recombination, which will be further explored with photoluminescence studies.

To explore the charge transfer from FTAZ to the acceptors, we measured the photoluminescence (PL) quenching of each blend (Fig. S11, ESI†). Both IDIC (Fig. S11a, ESI†) and IDTCF (Fig. S11c, ESI†) are able to quench the photoluminescence of FTAZ nearly completely (>95%), indicating efficient exciton dissociation in both blends. This suggests that a key step in charge generation, from exciton to the charge transfer (CT) state, is not a major issue in either the IDIC- or IDTCF-based device when FTAZ absorbs the incident photon. However, we cannot rule out the possibility of losing mobile charge carriers due to loss mechanisms including recombination to the ground state from the CT state.

Next, as both IDIC and IDTCF play a role in absorbing incident photons and thus generating excitons, we explore the

charge transfer from the acceptors to FTAZ through photoluminescence quenching as well. Unlike the previous case, there is a distinct difference in the PL quenching when looking at the acceptor excitation. To begin with, in the FTAZ:IDIC case (Fig. S11b, ESI†) there is strong quenching of the IDIC fluorescence by FTAZ ($\sim 90\%$). However, for FTAZ:IDTCF (Fig. S11d, ESI†) there is very poor quenching of the IDTCF fluorescence (\sim 20%). It is important to note that the overall PL of IDTCF is lower in Fig. S11 (ESI†) because of the excitation wavelength. For the excitation of the acceptor, a higher wavelength was needed to avoid any absorbance of the incident photons by FTAZ, therefore, just a shoulder of IDTCF was excited. The neat films of both IDIC and IDTCF display strong PL when excited at a more optimal wavelength, as demonstrated by their similar photoluminescence quantum efficiency (PLQE), which will be explored further in the next section. Most importantly, the inability of FTAZ to quench the photoluminescence of IDTCF suggests that geminate recombination is a major issue in the FTAZ:IDTCF blend.

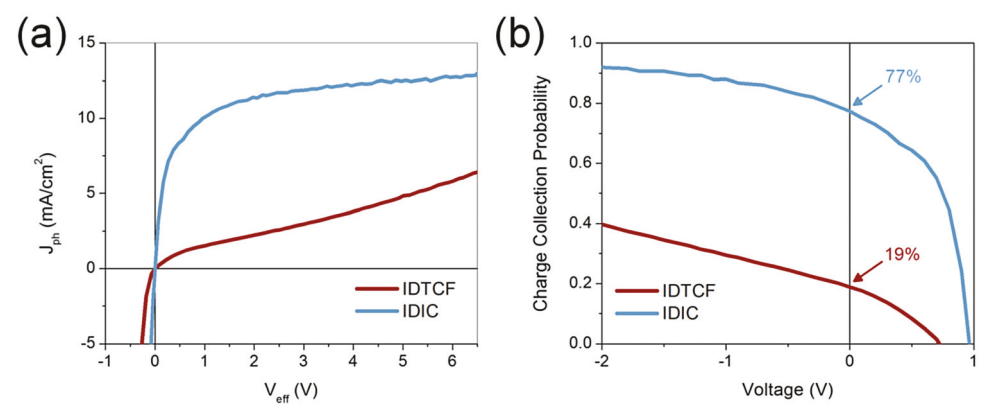
We also measured the PLQE for each of the materials. The PLQE is the quantum efficiency for the photoluminescence process (i.e., number of photons emitted/number of photons absorbed). In the case of neat IDIC and IDTCF, both have similar PLQE around 3%, as shown in Table S3 (ESI†). These values are appropriate for similar organic materials. Neat FTAZ films also have strong PL, but even lower PLQE (0.3%). The PL spectra for each are shown in Fig. S12 (ESI†). When looking at the blend films, FTAZ:IDIC has no PLQE, which further illustrates the strong quenching of FTAZ PL by IDIC; however, in the case of FTAZ:IDTCF, a PLQE similar to that of neat FTAZ is found (0.4%). This agrees with the poor quenching observed in the previously discussed PL experiments, and indicates that there may be an issue with charge transfer in the FTAZ:IDTCF system, which could lead to increased geminate recombination.

Through these photoluminescence experiments (summarized in Table 2), we have identified that geminate recombination may be a major issue for the FTAZ:IDTCF system. Therefore, while both FTAZ and IDTCF have the ability to absorb incident photons and generate excitons, there is not much interaction between the two materials, likely caused by the sterics of the IDTCF acceptor. Due to this lack of interaction, the excitons are more likely to undergo geminate recombination rather than splitting into free charge carriers, which would contribute to the much lower $J_{\rm sc}$ and FF measured for the IDTCF-based devices.

The poor packing and interaction observed in the FTA-Z:IDTCF system can also have an effect on the charge transport in the device. To explore the charge transport properties of

Table 2 Summary of photoluminescence studies

Blend	Photoluminescence quench efficiency@donor excitation	Photoluminescence quench efficiency@acceptor excitation	Photoluminescence quantum efficiency (PLQE)
FTAZ:IDIC	97.7%	89.4%	0.0%
FTAZ:IDTCF	95.5%	21.1%	0.4%



(a) Photocurrent density and (b) charge collection probability (P(E,T)) of FTAZ:IDIC and FTAZ:IDTCF based solar cells

these materials, we measured the mobility of the blends via the space charge limited current (SCLC) method. We have previously studied the hole and electron mobility for the FTAZ:IDIC blend, which were measured to be 1.5×10^{-4} and $2.6 \times 10^{-5} \text{ cm}^2 \text{ V}^{-1} \text{ s}^{-1}$, respectively.³⁹ For the IDTCF-based blend, hole- and electron-only devices were fabricated with the structure of ITO/PEDOT:PSS/FTAZ:IDTCF/MoO₃/Al and ITO/ZnO/ FTAZ:IDTCF/Ca/Al, respectively. The hole mobility of the FTAZ: IDTCF blend was measured to be 7.9×10^{-6} cm² V⁻¹ s⁻¹, which is over two orders of magnitude lower than the hole mobility generally observed for FTAZ-based blends. 39-42,69,70,79-81 Recall that the GIWAXS results found that IDTCF disrupts the packing of the FTAZ chains as seen by the larger (010) peak in the blend film. This effect will directly hinder the hole transport and would contribute to the low J_{sc} value observed for the FTAZ:IDTCF device. For the electron mobility, the measured dark current was extremely low, and a mobility value was not able to be determined (i.e., could not reach SCLC range). This implies that the electron transport is even more hindered than the hole transport, and the actual mobility value is likely of an even lower order of magnitude ($<10^{-6}$ cm² V⁻¹ s⁻¹). The poor electron transport could be due to the disrupted packing of IDTCF molecules, stemming from the steric hindrance imparted by the methyl groups on the TCF unit.

Finally, we studied the charge collection by looking at the charge collection probability (P(E,T)) for each blend (Fig. 5). Experimentally, the photocurrent density (J_{ph}) was first measured as a function of the effective voltage (V_{eff}) (Fig. 5a). 82 The photocurrent density is defined as the difference between the current densities in the dark and under illumination. The charge collection probability can then be calculated by dividing $J_{\rm ph}$ by the saturation photocurrent ($J_{\rm ph,sat}$). From Fig. 5a, it is clear that for the IDTCF-based device, the photocurrent continues to rise (i.e., doesn't saturate) even at high voltages (> 6 V), suggesting that charges are still being extracted. Generally, at higher applied voltages all generated excitons would split into free charge carriers which are subsequently collected at the electrodes, leading to a saturation of the photocurrent. The fact that charges are still not completely extracted at such high voltage values for the FTAZ:IDTCF device demonstrates the poor charge transfer that occurs in the devices containing IDTCF as an acceptor, which we have previously highlighted as a major issue in this system. Additionally, at the short-circuit condition, the IDIC-based device has a much higher P(E,T) than that of the IDTCF-based device, 77% vs. 19%, respectively (Fig. 5b). These results indicate that the charge collection process is far more efficient in the IDIC system. There have been multiple works that explore the effect of charge collection on device performance, and it has clearly been outlined that issues with charge collection results in $V_{\rm oc}$ loss. ^{77,83–85} Therefore, the low charge collection probability observed for the FTAZ:IDTCF device can also help explain the lower V_{oc} measured for this system compared to FTAZ:IDIC.

Conclusions

In summary, a hindered fused-ring electron acceptor, IDTCF, was developed to probe the impact of sterics at the acceptor end groups on the performance of non-fullerene acceptor (NFA) based BHJ solar cells. Compared to the control FREA of IDIC, IDTCF showed similar optical and electrochemical properties; however, the photovoltaic performance of IDTCF was ten times lower than that of IDIC. XRD, GIWAXS, and DFT calculations illustrated a difference in packing (π - π stacking) of these materials, and from a literature search of current high-performance FREAs, a common value of ~ 3.5 Å was found for $\pi - \pi$ stacking. GIWAXS measurements show that the IDTCF molecule has a larger π – π stacking distance of 4.40 Å compared to the 3.45 Å of IDIC. We identify geminate recombination and charge collection issues as the major mechanisms that cause the poor performance of the FTAZ:IDTCF system. Overall, these experiments provide a good explanation for the superior performance of IDIC-based devices compared to IDTCF. Particularly, we illustrated the importance of planarity of the end group acceptor moieties of FREAs, as even a methyl substituent out of the plane is enough to disrupt the packing and drastically decrease the device performance. Ultimately, this is one of the first works to concretely establish planarity and close packing as part of the design requirements for non-fullerene acceptors.

Author contributions

Jeromy J. Rech synthesized and characterized the FTAZ polymer and IDIC/IDTCF acceptors, collected NMR, MS, UV-vis, CV, PL, XRD data, and drafted the manuscript. Nicole Bauer fabricated and characterized solar cell devices, collected mobility measurements, light intensity, and charge collection probability data, and made samples for UV-Vis, PL, XRD, GIWAXS. David Dirkes and Joesph Kaplan synthesized various precursors for the IDIC and IDTCF acceptors. This work was all supervised under Prof. Wei You. Zhengxing Peng collected the GIWAXS data with help from Long Ye, under the guidance of Prof. Harald Ade. Huotian Zhang collected PLQE data, under the guidance of Prof. Feng Gao. Prof. Shubin Liu ran the computational work. All authors provided feedback on the manuscript and contributed to the editing and interpretation. Prof. Wei You directed this study.

Conflicts of interest

There are no conflicts to declare.

Acknowledgements

We thank the NSF (CBET-1639429) for financial support. We thank C. Donley for help with collecting the XRD data acquired at the Chapel Hill Analytical and Nanofabrication Laboratory, CHANL, a member of the North Carolina Research Triangle Nanotechnology Network, RTNN, which is supported by the National Science Foundation, Grant ECCS-1542015, as part of the National Nanotechnology Coordinated Infrastructure, NNCI. The authors thank the University of North Carolina's Department of Chemistry Mass Spectrometry Core Laboratory, especially B. Ehrmann, for their assistance with mass spectrometry analysis. We also thank S. Samson and the G. Meyer lab at UNC for assistance with the PL measurements. GIWAXS measurements and analysis are supported by ONR Grant No. N000141712204. GIWAXS data were acquired at beamline 7.3.3, at the Advanced Light Source (ALS) in Berkeley National Lab, which is supported by the U.S. Department of Energy (no. DE-AC02-05CH11231). S. Stuard assisted with part of the GIWAXS data acquisition. C. Zhu are acknowledged for beamline support at ALS.

References

- 1 H. Zhang, H. Yao, J. Hou, J. Zhu, J. Zhang, W. Li, R. Yu, B. Gao, S. Zhang and J. Hou, Over 14% Efficiency in Organic Solar Cells Enabled by Chlorinated Nonfullerene Small-Molecule Acceptors, Adv. Mater., 2018, 30, 1800613.
- 2 L. Meng, Y. Zhang, X. Wan, C. Li, X. Zhang, Y. Wang, X. Ke, Z. Xiao, L. Ding, R. Xia, H. Yip, Y. Cao and Y. Chen, Organic and solution-processed tandem solar cells with 17.3% efficiency, Science, 2018, 361, 1094-1098.
- 3 X. Che, Y. Li, Y. Qu and S. R. Forrest, High fabrication yield organic tandem photovoltaics combining vacuum- and solution-processed subcells with 15% efficiency, Nat. Energy, 2018, 3, 422-427.

- 4 Y. Zhang, B. Kan, Y. Sun, Y. Wang, R. Xia, X. Ke, Y.-Q.-Q. Yi, C. Li, H.-L. Yip, X. Wan, Y. Cao and Y. Chen, Nonfullerene Tandem Organic Solar Cells with High Performance of 14.11%, Adv. Mater., 2018, 30, 1707508.
- 5 Z. Xiao, X. Jia and L. Ding, Ternary organic solar cells offer 14% power conversion efficiency, Sci. Bull., 2017, 62, 1562-1564.
- 6 Z. Xiao, F. Liu, X. Geng, J. Zhang, S. Wang, Y. Xie, Z. Li, H. Yang, Y. Yuan and L. Ding, A carbon-oxygen-bridged ladder-type building block for efficient donor and acceptor materials used in organic solar cells, Sci. Bull., 2017, 62, 1331-1336.
- 7 B. Fan, D. Zhang, M. Li, W. Zhong, Z. Zeng, L. Ying, F. Huang and Y. Cao, Achieving over 16% efficiency for single-junction organic solar cells, Sci. China: Chem., DOI: 10.1007/s11426-019-9457-5.
- 8 J. Yuan, Y. Zhang, L. Zhou, G. Zhang, H.-L. Yip, T.-K. Lau, X. Lu, C. Zhu, H. Peng, P. A. Johnson, M. Leclerc, Y. Cao, J. Ulanski, Y. Li and Y. Zou, Single-Junction Organic Solar Cell with over 15% Efficiency Using Fused-Ring Acceptor with Electron-Deficient Core, Joule, 2019, 1-12.
- 9 X. Xu, T. Yu, Z. Bi, W. Ma, Y. Li and Q. Peng, Realizing Over 13% Efficiency in Green-Solvent-Processed Nonfullerene Organic Solar Cells Enabled by 1,3,4-Thiadiazole-Based Wide-Bandgap Copolymers, Adv. Mater., 2018, 30, 1703973.
- 10 X. Ma, W. Gao, J. Yu, Q. An, M. Zhang, Z. Hu, J. Wang, W. Tang, C. Yang and F. Zhang, Ternary nonfullerene polymer solar cells with efficiency >13.7% by integrating the advantages of the materials and two binary cells, *Energy* Environ. Sci., 2018, 11, 2134-2141.
- 11 Y. Lin, J. Wang, Z.-G. Zhang, H. Bai, Y. Li, D. Zhu and X. Zhan, An Electron Acceptor Challenging Fullerenes for Efficient Polymer Solar Cells, Adv. Mater., 2015, 27, 1170-1174.
- 12 B. Jia, S. Dai, Z. Ke, C. Yan, W. Ma and X. Zhan, Breaking 10% Efficiency in Semitransparent Solar Cells with Fused-Undecacyclic Electron Acceptor, Chem. Mater., 2018, 30, 239-245.
- 13 F. Zhao, S. Dai, Y. Wu, Q. Zhang, J. Wang, L. Jiang, Q. Ling, Z. Wei, W. Ma, W. You, C. Wang and X. Zhan, Single-Junction Binary-Blend Nonfullerene Polymer Solar Cells with 12.1% Efficiency, Adv. Mater., 2017, 29, 1700144.
- 14 Y. Lin and X. Zhan, Non-fullerene acceptors for organic photovoltaics: an emerging horizon, Mater. Horiz., 2014,
- 15 V. A. Trukhanov and D. Y. Paraschuk, Non-fullerene acceptors for organic solar cells, Polym. Sci., Ser. C, 2014, 56, 72-83.
- 16 S. Dai and X. Zhan, Nonfullerene Acceptors for Semitransparent Organic Solar Cells, Adv. Energy Mater., 2018, 1800002, 1-8.
- 17 T. Kietzke, Recent Advances in Organic Solar Cells, Adv. OptoElectron., 2007, 2007, 1-15.
- 18 D. He, F. Zhao, L. Jiang and C. Wang, A-D-A small molecule acceptors with ladder-type arenes for organic solar cells, J. Mater. Chem. A, 2018, 6, 8839-8854.
- 19 W. Huang, P. Cheng, Y. M. Yang, G. Li and Y. Yang, High-Performance Organic Bulk-Heterojunction Solar Cells Based on Multiple-Donor or Multiple-Acceptor Components, Adv. Mater., 2018, 30, 1705706.

- 20 R. Yu, H. Yao and J. Hou, Recent Progress in Ternary Organic Solar Cells Based on Nonfullerene Acceptors, Adv. Energy Mater., 2018, 1702814, 1702814.
- 21 F. Shen, J. Xu, X.-M. Li and C. Zhan, Nonfullerene small-molecule acceptors with perpendicular side-chains for fullerene-free solar cells, *J. Mater. Chem. A*, 2018, **6**, 15433–15455.
- 22 N. Qiu, H. Zhang, X. Wan, C. Li, X. Ke, H. Feng, B. Kan, H. Zhang, Q. Zhang, Y. Lu and Y. Chen, A New Nonfullerene Electron Acceptor with a Ladder Type Backbone for High-Performance Organic Solar Cells, Adv. Mater., 2017, 29, 1604964.
- 23 J. Zhu, Z. Ke, Q. Zhang, J. Wang, S. Dai, Y. Wu, Y. Xu, Y. Lin, W. Ma, W. You and X. Zhan, Naphthodithiophene-Based Nonfullerene Acceptor for High-Performance Organic Photovoltaics: Effect of Extended Conjugation, *Adv. Mater.*, 2018, 30, 1704713.
- 24 H. Yao, Y. Cui, R. Yu, B. Gao, H. Zhang and J. Hou, Design, Synthesis, and Photovoltaic Characterization of a Small Molecular Acceptor with an Ultra-Narrow Band Gap, *Angew. Chem.*, *Int. Ed.*, 2017, 56, 3045–3049.
- 25 H. Lu, J. Zhang, J. Chen, Q. Liu, X. Gong, S. Feng, X. Xu, W. Ma and Z. Bo, Ternary-Blend Polymer Solar Cells Combining Fullerene and Nonfullerene Acceptors to Synergistically Boost the Photovoltaic Performance, *Adv. Mater.*, 2016, 28, 9559–9566.
- 26 Y. Lin, Y. Jin, S. Dong, W. Zheng, J. Yang, A. Liu, F. Liu, Y. Jiang, T. P. Russell, F. Zhang, F. Huang and L. Hou, Printed Nonfullerene Organic Solar Cells with the Highest Efficiency of 9.5%, *Adv. Energy Mater.*, 2018, 8, 1701942.
- 27 X. Shi, L. Zuo, S. B. Jo, K. Gao, F. Lin, F. Liu and A. K.-Y. Jen, Design of a Highly Crystalline Low-Band Gap Fused-Ring Electron Acceptor for High-Efficiency Solar Cells with Low Energy Loss, *Chem. Mater.*, 2017, 29, 8369–8376.
- 28 Z. Luo, H. Bin, T. Liu, Z.-G. Zhang, Y. Yang, C. Zhong, B. Qiu, G. Li, W. Gao, D. Xie, K. Wu, Y. Sun, F. Liu, Y. Li and C. Yang, Fine-Tuning of Molecular Packing and Energy Level through Methyl Substitution Enabling Excellent Small Molecule Acceptors for Nonfullerene Polymer Solar Cells with Efficiency up to 12.54%, Adv. Mater., 2018, 30, 1706124.
- 29 L. Ye, Y. Xiong, Q. Zhang, S. Li, C. Wang, Z. Jiang, J. Hou, W. You and H. Ade, Surpassing 10% Efficiency Benchmark for Nonfullerene Organic Solar Cells by Scalable Coating in Air from Single Nonhalogenated Solvent, *Adv. Mater.*, 2018, 30, 1705485.
- 30 W. Zhao, S. Li, H. Yao, S. Zhang, Y. Zhang, B. Yang and J. Hou, Molecular Optimization Enables over 13% Efficiency in Organic Solar Cells, *J. Am. Chem. Soc.*, 2017, **139**, 7148–7151.
- 31 K. Jiang, G. Zhang, G. Yang, J. Zhang, Z. Li, T. Ma, H. Hu, W. Ma, H. Ade and H. Yan, Multiple Cases of Efficient Nonfullerene Ternary Organic Solar Cells Enabled by an Effective Morphology Control Method, *Adv. Energy Mater.*, 2018, **8**, 1701370.
- 32 J. Hou, O. Inganäs, R. H. Friend and F. Gao, Organic solar cells based on non-fullerene acceptors, *Nat. Mater.*, 2018, 17, 119–128.
- 33 X. Liu, Y. Yan, Y. Yao and Z. Liang, Ternary Blend Strategy for Achieving High-Efficiency Organic Solar Cells with

- Nonfullerene Acceptors Involved, Adv. Funct. Mater., 2018, 28, 1802004.
- 34 H. Yao, L. Ye, J. Hou, B. Jang, G. Han, Y. Cui, G. M. Su, C. Wang, B. Gao, R. Yu, H. Zhang, Y. Yi, H. Y. Woo, H. Ade and J. Hou, Achieving Highly Efficient Nonfullerene Organic Solar Cells with Improved Intermolecular Interaction and Open-Circuit Voltage, Adv. Mater., 2017, 29, 1700254.
- 35 H. Yao, Y. Chen, Y. Qin, R. Yu, Y. Cui, B. Yang, S. Li, K. Zhang and J. Hou, Design and Synthesis of a Low Bandgap Small Molecule Acceptor for Efficient Polymer Solar Cells, Adv. Mater., 2016, 28, 8283–8287.
- 36 S. Li, L. Ye, W. Zhao, X. Liu, J. Zhu, H. Ade and J. Hou, Design of a New Small-Molecule Electron Acceptor Enables Efficient Polymer Solar Cells with High Fill Factor, Adv. Mater., 2017, 29, 1704051.
- 37 Y. Cui, C. Yang, H. Yao, J. Zhu, Y. Wang, G. Jia, F. Gao and J. Hou, Efficient Semitransparent Organic Solar Cells with Tunable Color enabled by an Ultralow-Bandgap Nonfullerene Acceptor, Adv. Mater., 2017, 29, 1703080.
- 38 B. Kan, H. Feng, X. Wan, F. Liu, X. Ke, Y. Wang, Y. Wang, H. Zhang, C. Li, J. Hou and Y. Chen, Small-Molecule Acceptor Based on the Heptacyclic Benzodi-(cyclopentadithiophene) Unit for Highly Efficient Nonfullerene Organic Solar Cells, J. Am. Chem. Soc., 2017, 139, 4929–4934.
- 39 J. Zhu, Y. Wu, J. Rech, J. Wang, K. Liu, T. Li, Y. Lin, W. Ma, W. You and X. Zhan, Enhancing the performance of a fused-ring electron acceptor via extending benzene to naphthalene, *J. Mater. Chem. C*, 2018, 6, 66–71.
- 40 Z. Li, S. Dai, J. Xin, L. Zhang, Y. Wu, J. Rech, F. Zhao, T. Li, K. Liu, Q. Liu, W. Ma, W. You, C. Wang and X. Zhan, Enhancing the performance of the electron acceptor ITIC-Th via tailoring its end groups, *Mater. Chem. Front.*, 2018, 2, 537–543.
- 41 T. Li, H. Zhang, Z. Xiao, J. J. Rech, H. Niu, W. You and L. Ding, A carbon–oxygen-bridged hexacyclic ladder-type building block for low-bandgap nonfullerene acceptors, *Mater. Chem. Front.*, 2018, 2, 700–703.
- 42 P. Xue, J. Zhang, J. Xin, J. Rech, T. Li, K. Meng, W. Ma, W. You, M. R. Marder, R. P. S. Han and X. Zhan, Effects of Terminal Groups in Third Components on Performance of Organic Solar Cells, *Acta Phys. Chim. Sin.*, 2018, 34, 1–9.
- 43 S. Dai, F. Zhao, Q. Zhang, T.-K. Lau, T. Li, K. Liu, Q. Ling, C. Wang, X. Lu, W. You and X. Zhan, Fused Nonacyclic Electron Acceptors for Efficient Polymer Solar Cells, *J. Am. Chem. Soc.*, 2017, 139, 1336–1343.
- 44 J. Mai, Y. Xiao, G. Zhou, J. Wang, J. Zhu, N. Zhao, X. Zhan and X. Lu, Hidden Structure Ordering Along Backbone of Fused-Ring Electron Acceptors Enhanced by Ternary Bulk Heterojunction, *Adv. Mater.*, 2018, **30**, 1802888.
- 45 F. Liu, Z. Zhou, C. Zhang, J. Zhang, Q. Hu, T. Vergote, F. Liu, T. P. Russell and X. Zhu, Efficient Semitransparent Solar Cells with High NIR Responsiveness Enabled by a Small-Bandgap Electron Acceptor, Adv. Mater., 2017, 29, 1606574.
- 46 W. Gao, M. Zhang, T. Liu, R. Ming, Q. An, K. Wu, D. Xie, Z. Luo, C. Zhong, F. Liu, F. Zhang, H. Yan and C. Yang, Asymmetrical Ladder-Type Donor-Induced Polar Small

- Molecule Acceptor to Promote Fill Factors Approaching 77% for High-Performance Nonfullerene Polymer Solar Cells, Adv. Mater., 2018, 30, 1800052.
- 47 X. Shi, J. Chen, K. Gao, L. Zuo, Z. Yao, F. Liu, J. Tang and A. K.-Y. Jen, Terthieno[3,2-b]Thiophene (6T) Based Low Bandgap Fused-Ring Electron Acceptor for Highly Efficient Solar Cells with a High Short-Circuit Current Density and Low Open-Circuit Voltage Loss, Adv. Energy Mater., 2018, 8, 1702831.
- 48 H. Bin, L. Gao, Z.-G. Zhang, Y. Yang, Y. Zhang, C. Zhang, S. Chen, L. Xue, C. Yang, M. Xiao and Y. Li, 11.4% Efficiency non-fullerene polymer solar cells with trialkylsilyl substituted 2D-conjugated polymer as donor, Nat. Commun., 2016, 7, 13651.
- 49 J. Wang, W. Wang, X. Wang, Y. Wu, Q. Zhang, C. Yan, W. Ma, W. You and X. Zhan, Enhancing Performance of Nonfullerene Acceptors via Side-Chain Conjugation Strategy, Adv. Mater., 2017, 29, 1702125.
- 50 W. Liu, J. Zhang, Z. Zhou, D. Zhang, Y. Zhang, S. Xu and X. Zhu, Design of a New Fused-Ring Electron Acceptor with Excellent Compatibility to Wide-Bandgap Polymer Donors for High-Performance Organic Photovoltaics, Adv. Mater., 2018, 30, 1800403.
- 51 Z. Zheng, O. M. Awartani, B. Gautam, D. Liu, Y. Qin, W. Li, A. Bataller, K. Gundogdu, H. Ade and J. Hou, Efficient Charge Transfer and Fine-Tuned Energy Level Alignment in a THF-Processed Fullerene-Free Organic Solar Cell with 11.3% Efficiency, Adv. Mater., 2017, 29, 1604241.
- 52 S. Jie Xu, Z. Zhou, W. Liu, Z. Zhang, F. Liu, H. Yan and X. Zhu, A Twisted Thieno[3,4-b]thiophene-Based Electron Acceptor Featuring a 14-π-Electron Indenoindene Core for High-Performance Organic Photovoltaics, Adv. Mater., 2017, 29, 1704510.
- 53 Z. Zhang, M. Li, Y. Liu, J. Zhang, S. Feng, X. Xu, J. Song and Z. Bo, Simultaneous enhancement of the molecular planarity and the solubility of non-fullerene acceptors: effect of aliphatic side-chain substitution on the photovoltaic performance, J. Mater. Chem. A, 2017, 5, 7776-7783.
- 54 Z. Liang, M. Li, X. Zhang, Q. Wang, Y. Jiang, H. Tian and Y. Geng, Near-infrared absorbing non-fullerene acceptors with selenophene as π bridges for efficient organic solar cells, J. Mater. Chem. A, 2018, 6, 8059-8067.
- 55 Z. Zhang, J. Yu, X. Yin, Z. Hu, Y. Jiang, J. Sun, J. Zhou, F. Zhang, T. P. Russell, F. Liu and W. Tang, Conformation Locking on Fused-Ring Electron Acceptor for High-Performance Nonfullerene Organic Solar Cells, Adv. Funct. Mater., 2018, 28, 1705095.
- 56 T. Li, S. Dai, Z. Ke, L. Yang, J. Wang, C. Yan, W. Ma and X. Zhan, Fused Tris(thienothiophene)-Based Electron Acceptor with Strong Near-Infrared Absorption for High-Performance As-Cast Solar Cells, Adv. Mater., 2018, 30, 1705969.
- 57 L. Ye, W. Zhao, S. Li, S. Mukherjee, J. H. Carpenter, O. Awartani, X. Jiao, J. Hou and H. Ade, High-Efficiency Nonfullerene Organic Solar Cells: Critical Factors that Affect Complex Multi-Length Scale Morphology and Device Performance, Adv. Energy Mater., 2017, 7, 1602000.

- 58 J. Zhang, C. Yan, W. Wang, Y. Xiao, X. Lu, S. Barlow, T. C. Parker, X. Zhan and S. R. Marder, Panchromatic Ternary Photovoltaic Cells Using a Nonfullerene Acceptor Synthesized Using C-H Functionalization, Chem. Mater., 2018, 30,
- 59 W. Wang, C. Yan, T.-K. Lau, J. Wang, K. Liu, Y. Fan, X. Lu and X. Zhan, Fused Hexacyclic Nonfullerene Acceptor with Strong Near-Infrared Absorption for Semitransparent Organic Solar Cells with 9.77% Efficiency, Adv. Mater., 2017, 29, 1701308.
- 60 H. Feng, N. Qiu, X. Wang, Y. Wang, B. Kan, X. Wan, M. Zhang, A. Xia, C. Li, F. Liu, H. Zhang and Y. Chen, An A-D-A Type Small-Molecule Electron Acceptor with End-Extended Conjugation for High Performance Organic Solar Cells, Chem. Mater., 2017, 29, 7908-7917.
- 61 H. Hu, K. Jiang, P. C. Y. Chow, L. Ye, G. Zhang, Z. Li, J. H. Carpenter, H. Ade and H. Yan, Influence of Donor Polymer on the Molecular Ordering of Small Molecular Acceptors in Nonfullerene Polymer Solar Cells, Adv. Energy Mater., 2018, 8, 1701674.
- 62 Q. Fan, Y. Wang, M. Zhang, B. Wu, X. Guo, Y. Jiang, W. Li, B. Guo, C. Ye, W. Su, J. Fang, X. Ou, F. Liu, Z. Wei, T. C. Sum, T. P. Russell and Y. Li, High-Performance As-Cast Nonfullerene Polymer Solar Cells with Thicker Active Layer and Large Area Exceeding 11% Power Conversion Efficiency, Adv. Mater., 2018, 30, 1704546.
- 63 Y. Chen, P. Ye, X. Jia, W. Gu, X. Xu, X. Wu, J. Wu, F. Liu, Z. Zhu and H. Huang, Tuning V oc for high performance organic ternary solar cells with non-fullerene acceptor alloys, J. Mater. Chem. A, 2017, 5, 19697-19702.
- 64 X. Li, T. Yan, H. Bin, G. Han, L. Xue, F. Liu, Y. Yi, Z.-G. Zhang, T. P. Russell and Y. Li, Insertion of double bond π-bridges of A-D-A acceptors for high performance nearinfrared polymer solar cells, J. Mater. Chem. A, 2017, 5, 22588-22597.
- 65 L. Yang, W. Gu, L. Hong, Y. Mi, F. Liu, M. Liu, Y. Yang, B. Sharma, X. Liu and H. Huang, High Performing Ternary Solar Cells through Förster Resonance Energy Transfer between Nonfullerene Acceptors, ACS Appl. Mater. Interfaces, 2017, 9, 26928-26936.
- 66 M. He, T. M. Leslie and J. A. Sinicropi, α-Hydroxy ketone precursors leading to a novel class of electro-optic acceptors, Chem. Mater., 2002, 14, 2393-2400.
- 67 S. C. Price, A. C. Stuart, L. Yang, H. Zhou and W. You, Fluorine Substituted Conjugated Polymer of Medium Band Gap Yields 7% Efficiency in Polymer-Fullerene Solar Cells, J. Am. Chem. Soc., 2011, 133, 4625-4631.
- 68 A. Hexemer, W. Bras, J. Glossinger, E. Schaible, E. Gann, R. Kirian, A. MacDowell, M. Church, B. Rude and H. Padmore, A SAXS/WAXS/GISAXS Beamline with Multilayer Monochromator, J. Phys.: Conf. Ser., 2010, 247, 012007.
- 69 D. He, F. Zhao, J. Xin, J. J. Rech, Z. Wei, W. Ma, W. You, B. Li, L. Jiang, Y. Li and C. Wang, A Fused Ring Electron Acceptor with Decacyclic Core Enables over 13.5% Efficiency for Organic Solar Cells, Adv. Energy Mater., 2018, 8, 1802050.

- 70 S. Dai, Y. Xiao, P. Xue, J. James Rech, K. Liu, Z. Li, X. Lu, W. You and X. Zhan, Effect of Core Size on Performance of Fused-Ring Electron Acceptors, Chem. Mater., 2018, 30, 5390-5396.
- 71 U. Würfel, D. Neher, A. Spies and S. Albrecht, Impact of charge transport on current-voltage characteristics and power-conversion efficiency of organic solar cells, Nat. Commun., 2015, 6, 6951.
- 72 M. Stolterfoht, A. Armin, B. Philippa and D. Neher, The Role of Space Charge Effects on the Competition between Recombination and Extraction in Solar Cells with Low-Mobility Photoactive Layers, *J. Phys. Chem. Lett.*, 2016, 7, 4716–4721.
- 73 D. Neher, J. Kniepert, A. Elimelech and L. J. A. Koster, A New Figure of Merit for Organic Solar Cells with Transportlimited Photocurrents, Sci. Rep., 2016, 6, 24861.
- 74 L. Lu, T. Zheng, T. Xu, D. Zhao and L. Yu, Mechanistic Studies of Effect of Dispersity on the Photovoltaic Performance of PTB7 Polymer Solar Cells, Chem. Mater., 2015, 27, 537-543.
- 75 S. Solak, P. W. M. Blom and G. A. H. Wetzelaer, Effect of non-ohmic contacts on the light-intensity dependence of the open-circuit voltage in organic solar cells, Appl. Phys. Lett., 2016, 109, 053302.
- 76 S. R. Cowan, A. Roy and A. J. Heeger, Recombination in polymer-fullerene bulk heterojunction solar cells, Phys. Rev. B: Condens. Matter Mater. Phys., 2010, 82, 245207.
- 77 A. K. K. Kyaw, D. H. Wang, V. Gupta, W. L. Leong, L. Ke, G. C. Bazan and A. J. Heeger, Intensity Dependence of Current-Voltage Characteristics and Recombination in High-Efficiency Solution-Processed Small-Molecule Solar Cells, ACS Nano, 2013, 7, 4569-4577.
- 78 V. V. Brus, Light dependent open-circuit voltage of organic bulk heterojunction solar cells in the presence of surface recombination, Org. Electron., 2016, 29, 1-6.

- 79 Q. Zhang, L. Yan, X. Jiao, Z. Peng, S. Liu, J. J. Rech, E. Klump, H. Ade, F. So and W. You, Fluorinated Thiophene Units Improve Photovoltaic Device Performance of Donor-Acceptor Copolymers, Chem. Mater., 2017, 29, 5990-6002.
- 80 N. Bauer, Q. Zhang, J. J. Rech, S. Dai, Z. Peng, H. Ade, J. Wang, X. Zhan and W. You, The impact of fluorination on both donor polymer and non-fullerene acceptor: The more fluorine, the merrier, Nano Res., DOI: 10.1007/s12274-019-2362-3.
- 81 J. Wang, Y. Xiao, W. Wang, C. Yan, J. Rech, M. Zhang, W. You, X. Lu and X. Zhan, Pairing 1D/2D-conjugation donors/acceptors towards high-performance organic solar cells, Mater. Chem. Front., 2019, 3, 276-283.
- 82 L. Yang, J. R. Tumbleston, H. Zhou, H. Ade and W. You, Disentangling the impact of side chains and fluorine substituents of conjugated donor polymers on the performance of photovoltaic blends, Energy Environ. Sci., 2013, 6, 316-326.
- 83 H. Cha, S. Wheeler, S. Holliday, S. D. Dimitrov, A. Wadsworth, H. H. Lee, D. Baran, I. McCulloch and J. R. Durrant, Influence of Blend Morphology and Energetics on Charge Separation and Recombination Dynamics in Organic Solar Cells Incorporating a Nonfullerene Acceptor, Adv. Funct. Mater., 2018, 28, 1704389.
- 84 H. Cha, C.-H. Tan, J. Wu, Y. Dong, W. Zhang, H. Chen, S. Rajaram, K. S. Narayan, I. McCulloch and J. R. Durrant, An Analysis of the Factors Determining the Efficiency of Photocurrent Generation in Polymer:Nonfullerene Acceptor Solar Cells, Adv. Energy Mater., 2018, 8, 1801537.
- 85 J. Hong, M. J. Sung, H. Cha, C. E. Park, J. R. Durrant, T. K. An, Y.-H. Kim and S.-K. Kwon, Understanding Structure-Property Relationships in All-Small-Molecule Solar Cells Incorporating a Fullerene or Nonfullerene Acceptor, ACS Appl. Mater. Interfaces, 2018, 10, 36037-36046.